

# Thermal expansion properties of metallic and cermet coatings

J. Ilavsky<sup>1</sup>, C.C. Berndt<sup>\*</sup>

*The Center for Thermal Spray Research, SUNY at Stony Brook, 306 Old Engineering Stony Brook, NY 11794-2275, USA*

Received 20 February 1997; accepted 5 August 1997

## Abstract

Free-standing deposits of NiCrAl, stainless steel, and 8 wt.% yttria-stabilized zirconia were prepared using atmospheric plasma spraying and high velocity oxygen fuel processing. Feedstock powders were blended, yielding mixtures (by weight) of 100%, 75%, and 50% of the metallic material. Porosity and composition (i.e. metal or ceramic constituents) of these deposits were measured by image analysis.

The coefficient of thermal expansion (CTE) was measured in the 200–950 °C interval for four thermal cycles. The first runs of these CTE measurements were not linear and differentiation of this curve established the CTE dependence with respect to temperature. Maximums in CTE behavior suggest that stress relaxation and/or oxidation may be occurring. Measurements of CTE from thermal cycles after the first cycle were constant and obeyed the law of mixtures in the measured temperature region, suggesting that stress relaxation and/or oxidation, evident in the first cycle, are no longer dominant. Microstructural analysis and microhardness measurements were used to confirm the findings from CTE measurements. © 1998 Elsevier Science S.A.

*Keywords:* Cermet coatings; Thermal expansion; Thermal spray processes; Stress relaxation

## 1. Introduction

Thick thermal barrier coatings (TTBCs) for diesel engines operating in the 400 to 800 °C region have been extensively studied [1–3]. Such comparatively low-temperature applications for deposits are different from thermal barrier coatings (TBCs) that are used in the 1100 °C range for gas turbine engines. For instance, TTBCs are usually manufactured with compositions varying from 100% metal (as the bond coat) to 100% ceramic (as the top coat) with intermediate cermet layers, so that the overall thickness may be in the order of 5 mm. The thermal conductivity of the deposit system can be decreased by employing higher porosity deposits, but this may lead to increased gas permeability, which increases requirements on the oxidation resistance of the metallic material.

An important feature of metallic and cermet deposits is the stress within the deposit after spray processing as well as the stress created during service. The magnitude of stress associated with plasma spray deposition

depends on the temperature history during the processing, on the thermal expansion coefficients, and on the elastic properties of the sprayed material and the substrate [4,5]. Therefore, processes such as atmospheric plasma spraying (APS) and high velocity oxygen fuel (HVOF) spraying, and various spray material compositions result in different stresses. Stresses in the metallic and cermet deposits are related to oxidation during the service life of the deposit [6]. Since the oxide volume is generally greater than that of the original metal, the deposit volume will be expected to increase with oxidation [7].

The thermal cycling of graded coating systems (consisting of layers which exhibit different intrinsic thermal expansion coefficients) results in stress changes during heating and cooling. Stress relaxation measurement techniques have been developed for different samples; however, stresses associated with plasma-sprayed deposits are still difficult to assess. Some studies used the bending of the deposit/substrate system after the spray process [8,9]. Other possibilities include destructive techniques, such as hole-drilling and polishing methods [10], and X-ray or neutron diffraction. Measurements for plasma-sprayed deposits have seldom been successful, probably due to their complex microstructure.

It has been proposed [11] that microhardness changes

<sup>\*</sup> Corresponding author. Fax: (+ 1) 516 632 8052;

e-mail: cberndt@cmail.sunysb.edu

<sup>1</sup> Present address: The Institute of Plasma Physics, Prague. The Czech Republic.

are indicative of microstructural processes occurring within deposits during heat treatment. If other processes such as phase transformations are controlled, then stress relaxation (or, more generally, stress redistribution, since stresses are inherent to as-sprayed materials) and build up can be assessed using microhardness measurements. The influence of the stress relaxation should manifest itself in lowering the deposit's material variability since parts of the deposit originally under different stress conditions attain similar stress levels. This results in a decrease of the standard deviation, which is equivalent to an increase of Weibull modulus. Changes in the average microhardness depend on the material processes and may be different from material to material. For example, if the sample is originally under compressive stress, then stress relaxation should reduce the average microhardness.

Anisotropy and deviations from linearity of the coefficient of thermal expansion (CTE) are useful for measuring material characteristics within deposits [12] which include processes such as phase transformations, stress relaxation, and oxidation. If stress relaxation in the deposit is a thermally activated process, then a maximum or minimum would be expected in the CTE vs. temperature curve. The relaxation processes would be related to material changes such as phase changes, dislocation movement, grain growth and grain boundary reorientation or crack propagation, and diffusion. It is difficult to detail the dominant mechanisms from thermal expansion; however, it can be expected that there would be a combination of many mechanisms.

Volume increase arising from oxidation will also result in non-linear thermal expansion changes. The low-to-medium temperature oxidation properties of materials containing elements such as Al, Cr, Ni, and Co, will be complex, since each element will be active over various temperature regions [7]. Oxidation behavior also depends on the surface area and gas permeability of the deposits, and these microstructural features are expected to be of special significance for cermet deposits. Oxidation will continue rapidly until all exposed metal is covered by an oxide layer. Continuation of oxidation after this stage depends on the mechanical behavior of the oxide scales and their relationship to surrounding lamellae during thermal cycling. The CTE vs. temperature curve allows estimation of the starting and maximum temperatures of oxidation processes.

## 2. Materials and processing

Metallic materials of NiCrAl<sup>2</sup> (Metco 443 consisting of 75% Ni, 19% Cr, 6% Al) and stainless steel (Metco 41 F-NS, austenitic stainless steel consisting of 64.6%

Fe, 17.1% Cr, 13% Ni, 2.2% Mo, <2.2% Mn, <1.0% Si, <0.10% C) were used. Deposits were prepared from 100% metal material and from powder mixtures of 75% and 50% of metal blended with a balance of yttria-stabilized zirconia (YSZ) ceramic (Muscle Shoals Minerals ZY8 consisting of ZrO<sub>2</sub>+8 wt.% Y<sub>2</sub>O<sub>3</sub>). The deposits were prepared by conventional plasma spraying with a Metco 3MB gun and by HVOF spraying with the Jet Kote<sup>™</sup> process. Deposits of 1 mm (0.04 in) thickness were sprayed onto a smooth steel substrate and then removed. Care was taken to avoid deformation in the deposit during stripping since this would change the stress state. Samples 8 mm wide and between 20 and 25 mm long were cut from these deposits for the thermal expansion measurements. Metallographic cross-sections were prepared for the structural studies and X-ray diffraction (XRD) was performed with a Phillips diffractometer equipped with Cu K $\alpha$  radiation. The deposit structure was examined by optical metallography, in which the microscope was connected to an image analysis system (Buehler Omnimet I). The system has a resolution of about 1  $\mu$ m at 200 $\times$  magnification and was used to measure the ceramic-to-metal ratio as well as the deposit porosity.

The thermal expansion measurements were carried out using a Theta dilatometer of 0.0022 mm precision; used at heating and cooling rates of 200 °C h<sup>-1</sup>. The temperature cycle was repeated at least four times between 200 °C and 950 °C and data collected at about every 20 °C. After differentiation of elongation over this 20 °C interval, the data were smoothed over intervals of 60 °C.

Two samples which exhibited extremes in thermal expansion behavior were selected for microhardness measurements under 500 g loads. The 100% HVOF-processed NiCrAl coating exhibited a large CTE peak associated with stress relaxation at 580 °C, whereas the APS-processed cermet of 75% stainless steel–25% YSZ exhibited a CTE peak associated with oxidation at –790 °C. (Refer to Fig. 2 (curve 4) and Fig. 4 (curve 5) respectively. This data will be formally presented in Section 3.) The samples were tested in as-sprayed conditions, as well as after heat treatment at 800 °C for 100 h.

The hardness results were processed using analyses based on Gaussian and Weibull statistics (using the maximum likelihood method [13]). There is an implicit assumption in such an analysis that the flaw size distribution is unimodal, and while this is true for the separate distributions of (i) interlamellar porosity and (ii) vertical cracks, it should be kept in mind that these distributions are platykurtic (i.e. flat) and that the combined effect of void distribution may not be ideally unimodal. (Thus porosity and cracks can both contribute to the total void distribution of the material.) However, since the indenter orientation during the hardness test will always be oriented preferentially with respect to only one of

<sup>2</sup>All compositions in weight percent.

these distributions then the measured material property will be largely influenced by only one of the void distributions. Thus a unimodal assumption on the material property, although not entirely accurate in the microstructural sense, is reasonable from the viewpoint of describing how the principle stress of the indenter interacts with the material.

### 3. Results and discussion

Structural characteristics of the six APS and six HVOF samples are detailed in Table 1. Note that the starting compositions of the blended materials, as indicated in the second column of Table 1, are often not reproduced by the measurements from the image analysis system (column 3) because the ceramic component exhibits a different deposition efficiency than the metal. The first run of some of the samples did not exhibit a linear elongation dependence with respect to temperature, Figs. 1-4. This behavior was reproducible for a given sample. The subsequent cycles (the CTEs are summarized in column 6 of Table 1) exhibit linear behavior and suggest that processes active in the first cycle are no longer operative. Thus process-induced stresses are relaxed during the first cycle, and/or oxide scales which protect the metal are created on all the available surfaces of the deposit. Thermal cycling did not give rise to any phase transformations that could be detected by XRD.

The coefficient of thermal expansion in cycles 2 to 4 was linear with respect to the temperature and fulfilled the law of mixtures with respect to the volume ratio of the ceramic and metal, Fig. 5. It can be seen that the CTE of the 100% ceramic material, as found by extrapolating to 0% metal, is about  $10.5 \times 10^{-6} \text{ K}^{-1}$ , which corresponds to literature values [12]. The different compositions of the deposits will be discussed in turn.

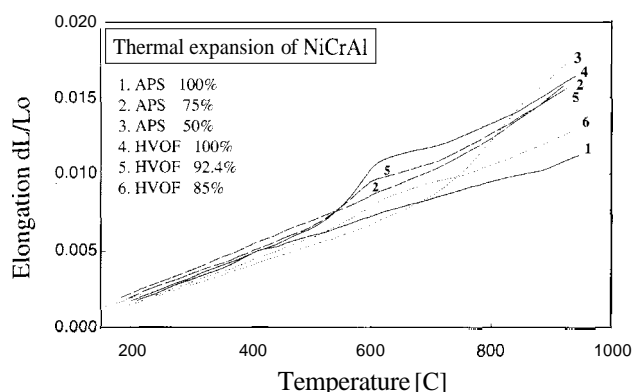


Fig. 1. Thermal expansion of NiCrAl-based materials during the first thermal cycle.

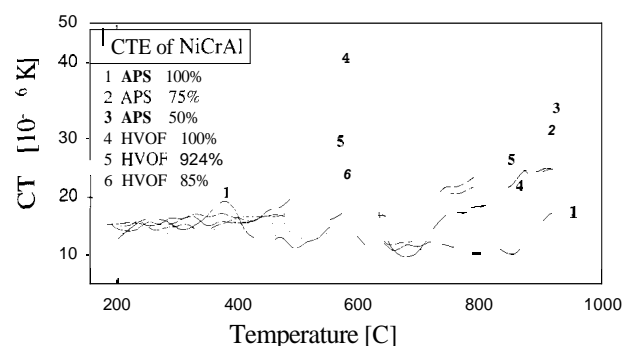


Fig. 2. Differential thermal expansion of NiCrAl-based materials during the first thermal cycle.

Table 1  
Image analysis and thermal expansion results

Code"	Feedstock composition	Ceramic content (error) (wt.%)	Metal content (error) (wt.%)	Porosity (error) (vol%)	CTE <sup>b</sup> in cycles 2 to 4 ( $10^{-6} \text{ K}^{-1}$ )
APS process					
1	100% NiCrAl	0	100	2.8 (1.0)	16.4
2	75% NiCrAl	25 (3)	75 (3)	3.4 (0.3)	15.4
3	50% NiCrAl	50 (2)	50 (2)	7.3 (0.8)	12.9
1	100% stainless steel	0	100	1.8 (0.7)	17.9
2	75% stainless steel	31 (2)	69 (2)	1.1 (0.4)	16.5
3	50% stainless steel	49 (2)	51 (2)	2.3 (0.5)	14.0
HVOF process					
4	100% NiCrAl	0	100	1.7 (0.7)	16.3
5	75% NiCrAl	8 (2)	92 (2)	0.8 (0.4)	15.7
6	50% NiCrAl	15 (2)	85 (2)	0.8 (0.3)	15.3
4	100% stainless steel	0	100	0.6 (0.1)	16.8
5	75% stainless steel	N/A	N/A	0.1 (0.1)	16.7
6	50% stainless steel	N/A	N A	0.2 (0.1)	16.7

<sup>a</sup> This code is used to identify the samples in Figs. 1-4. The duplicate codes are based on two different materials; there are six samples in each set of NiCrAl- and stainless-steel-based materials.

<sup>b</sup> Average of at least three runs; estimated error in the CTE measurements is  $0.2 \times 10^{-6} \text{ K}^{-1}$ .

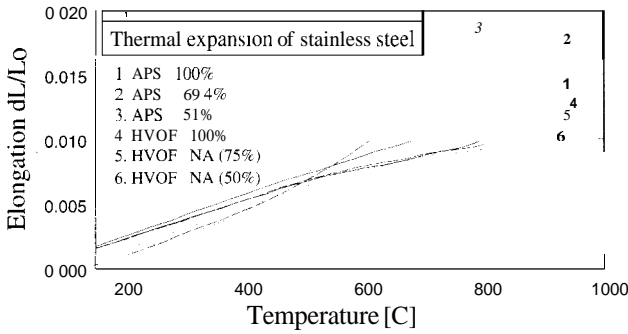


Fig. 3. Thermal expansion of stainless-steel-based materials during the first thermal cycle. Ceramic content of the HVOF-prepared samples was not measured (see text).

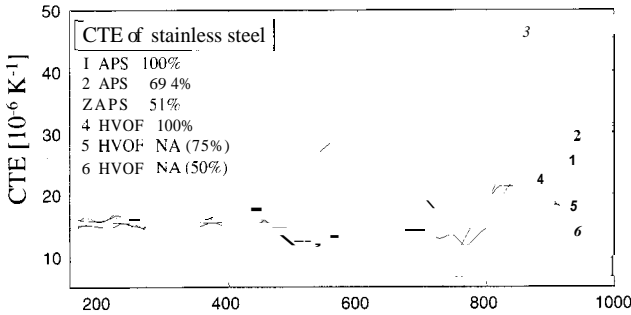


Fig. 4. Differential thermal expansion of stainless-steel-based materials during the first thermal cycle. Ceramic content of the HVOF-prepared samples was not measured (see text).

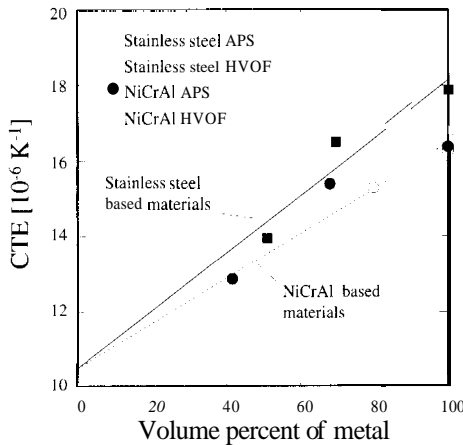


Fig. 5. Average thermal expansion of materials in cycles 2 to 4.

3.1. NiCrAl-based deposits

The different behavior of the HVOF-processed deposits compared with the APS materials can be seen in Figs. 1 and 2. The HVOF-processed samples (codes 4, 5, and 6) exhibit a large CTE at around 575 °C. The height of this increase is as much as 300% greater than the CTE of the APS metal deposit and decreases as the metal fraction increases. This phenomenon is manifested on the derivative curve by the presence of peaks (see

Fig. 2, curves 4–6) with changing height. Of the APS-processed materials, only the 100% metal deposit (curve 1) exhibits a peak similar to the HVOF-processed materials, and this appears at around 380 °C, although this peak loses its prominence when it is considered that the absolute error in the CTE measurement is  $-0.2 \times 10^{-6} \text{ K}^{-1}$ . All these peaks can be approximated by distribution curves which exhibit one maximum and a smooth shape. A trend is observed where materials with more ceramic exhibit a lower intensity peak; e.g. compare sample 6 to samples 5 and 4.

Both the APS and HVOF-processed materials exhibit an increase in CTE response at high temperatures; however, the character of curve 3 (the 50/50 mix which was APS-processed) can be distinguished since it exhibits an increase in CTE at low temperatures (about 650 °C) and, as well, the increase in CTE with respect to temperature is large. The peak of this curve is also broader and, unlike the other materials, exhibits a constant maximum CTE section over a 50 °C interval.

XRD and optical microscopy of cross-sections were performed on samples heat treated at 400, 600, and 800 °C. The results imply that the CTE peaks for the HVOF deposits and the 100% metal APS deposit arise from the relaxation of compressive stresses, since no extensive oxide changes were found that would suggest oxidation mechanisms. The 50% APS-processed deposit exhibits rapid oxidation at the 800 °C heat treatment, indicating that the extended flat peak in curve 3 (Fig. 2), which starts at around 620 °C, might be associated with deposit oxidation. The degree of oxidation and the oxidation rate would be enhanced because the small metal constituents are isolated within a porous ceramic that exhibits a high transport coefficient to oxygen. On the other hand, the APS 100% deposit would not be so susceptible to oxidation processes because of a lower void content and a reduced oxygen pressure arising from an oxygen gettering process in the surface regions of the deposit.

The HVOF process is particularly susceptible to high stress states since the powdered materials are subjected to high impact velocities at relatively low temperatures. Conversely, the plasma spraying process undergoes lower velocities at higher temperatures and, therefore, it would be expected for the deposit material to be more likely to undergo self-annealing and stress relaxation.

The thermal energy necessary for stress release is indicated by the temperature of the peak maximum in Fig. 2. The magnitude of the stress depends on the ceramic/metal ratio in the case of HVOF deposits. However, the temperature of the maximum is not dependent on the ceramic/metal ratio, suggesting that the relaxation mechanism does not change. The APS 100% metal deposit (curve 1) relaxes at a different temperature and is probably due to a different stress relaxation process.

### 3.2. Stainless-steel-based deposits

The results for the stainless steel samples are presented in Figs. 3 and 4. The APS-prepared cermet deposits exhibit a very broad peak in the derivative (CTE/temperature) curve starting at around 400 °C, with a maximum at around 600 °C. These peaks, as indicated by the XRD and optical microscope studies of the heat-treated samples, correspond to oxidation. Oxidation susceptibility is most prominent for the deposits containing most ceramic (49%) and sprayed by APS. The second most susceptible deposit is the 31% ceramic APS-processed deposit. These results are consistent with the trends observed for the NiCrAl-based materials; however, the stainless steel oxidizes at lower temperatures than the NiCrAl (as would be expected) and, therefore, the oxidation-induced effects on the CTE appear at a lower temperature; i.e.  $-875^{\circ}\text{C}$  for the APS 100% NiCrAl (Fig. 2, curve 1) compared with  $\sim 790^{\circ}\text{C}$  for the APS 100% stainless steel (Fig. 4, curve 1) and  $\sim 800^{\circ}\text{C}$  for the APS 50% NiCrAl (Fig. 2, curve 3) and  $\sim 600^{\circ}\text{C}$  for the APS 51% stainless steel (Fig. 4, curve 3).

The stainless steel materials prepared by HVOF cannot be compared in the same fashion as the NiCrAl-based deposits. The reason for this is that the image analysis results on the ceramic/metal ratio are not available since the ceramic constituent in the deposit could not be reliably identified. The CTE results in thermal cycles 2 to 4 are essentially the same (Table 1 and Fig. 3) and indicate that there is little ceramic in the cermet deposits. This occurs since the ceramic particles were not melted during the HVOF processing and, therefore, rebounded from the substrate, as was confirmed with very low deposition efficiencies for this material. The HVOF 100% stainless steel did not exhibit any stress relaxation, at least as measured from the CTE response. This may be due to (i) the lower intrinsic strength of the stainless steel or that (ii) stress relief occurs at the temperatures experienced during the HVOF process.

### 3.3. Microhardness measurement

The microhardness results are presented in Table 2 and the Weibull modulus data are shown in Fig. 6. In general, the microhardness depends on an intrinsic mate-

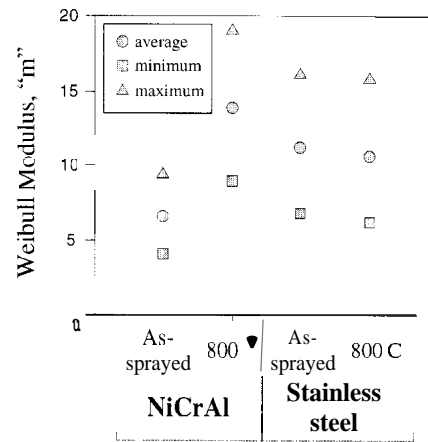


Fig. 6. Variation (Weibull modulus) of microhardness measurements for selected samples. Minimum and maximum values are a measure of error of the average value (90% probability calculated using maximum likelihood method).

rial property, the stress state of the material, the deposit density and the microstructure which includes the oxide content. It was not the intent of the present work to deconvolute all of these individual effects, but rather to assess the deposit response assuming that the prime factors, at least for the materials used in this study, were residual stress and oxide content.

The nickel-based sample exhibited a decrease in the average microhardness and standard deviation of microhardness, as well as an increase in the Weibull modulus after heat treatment. The stresses inherent in the as-received material relax after heat treatment and result in microstructural homogenization and a decrease in microhardness. The stainless steel sample showed opposite trends, i.e. an increase in microhardness and standard deviation with heat treatment. The Weibull moduli of the stainless steel samples did not change significantly, indicating that the dominating processes in this material during heat treatment are of a different nature than in the NiCrAl deposits.

The increase in the microhardness relates to oxidation of the sample as verified by optical microscopy. Oxidation creates brittle inclusions in the deposit which increase the microhardness of the deposit. The microhardness variability of the as-sprayed and heat-treated stainless steel–YSZ samples, at least as indicated by the Weibull modulus, was  $\sim 11$  units. This is significantly

Table 2  
Microhardness measurements of selected samples

Sample	HVN (standard deviation)	Weibull modulus (maximum likelihood)	Minimum HVN	Maximum HVN
100% NiCrAl, HVOF as-sprayed	305 (54)	6.6 (4.1–9.4)	213	412
100% NiCrAl, HVOF, 800 °C heat treated	275 (20)	13.9 (9.0–9.0)	244	323
75% stainless steel–25% YSZ, APS as-sprayed	299 (29)	11.2 (6.8–16.1)	255	356
75% stainless steel–25% YSZ, APS 800 °C heat treated	360 (45)	10.6 (6.2–15.8)	261	420

higher than for the as-sprayed NiCrAl sample ( $-7$  units) but slightly lower than the heat-treated NiCrAl material ( $-14$  units).

#### 4. Summary

Thermal expansion measurements are a useful tool to assess stress content and/or oxidation behavior of deposits. The character of the CTE temperature dependencies can be used to distinguish between oxidation and stress relaxation related processes if other microstructural determinations, such as image analysis and XRD, are also performed. This conclusion is also supported by the microhardness measurements, since the material properties and their variability were measured directly.

The processing technique and the material composition influence the stress content in deposits and also affect the oxidation resistance of the deposits. The NiCrAl-based deposits contain intrinsic compressive stresses if prepared by HVOF processing; the level of these stresses decreases rapidly when ceramic is blended into the feedstock material. The stresses were released at  $-575$  °C. for a heating rate of  $200$  °C h<sup>-1</sup> in the dilatometer. The APS 100% NiCrAl deposit exhibits little stress relaxation at around  $380$  °C and the APS cermet deposits exhibit no stress relaxation.

The stainless steel-based deposits are the most susceptible to oxidation-induced changes at temperatures  $<600$  °C. However, above  $600$  °C the APS 50% NiCrAl and the APS 75% NiCrAl-based cermets exhibit CTE responses that are related to oxidation. The oxidation of the APS 50% ceramic deposit starts at  $620$  °C. No stress relaxation effects were found for stainless steel deposits prepared by either the APS or HVOF processes. APS stainless steel cermet deposits are highly susceptible to oxidation, and this is directly proportional to the ceramic content. Thus, a deposit with an increase in ceramic content exhibits greater oxidation since the specific surface area of the metal component per unit volume of cermet is greater. HVOF processing was not

suitable for spraying cermet blends, at least for the ceramic of the particle size used in this work. Therefore, special cuts of ceramic feedstocks need to be tailored for HVOF processing and such specialized powders are currently finding applications.

#### Acknowledgement

This project has been supported under DOE sub-contract 85X-SH399C and NSF-MRSEC Program DMR 9632570. We thank Mr. G.A. Bancke for spraying our samples. The authors also gratefully acknowledge pertinent contributions from an anonymous reviewer.

#### References

- [1] M.B. Beardsley, in: E.W. Gregory, E.E. Wells Jr. (Eds.), Proc. 1990 Deposits for Advanced Heat Engines Workshop, Aug. 6–9, 1990. Maine Maritime Academy, Castine, ME. DOE, Washington, DC, 1990. Paper 11-53.
- [2] R.A. Miller. DOE NASA 21749-1. 1990.
- [3] R.C. Novak, A.P. Matarese, R.P. Huston, A.J. Scharman, T.M. Yonushonis, Mater. Manuf. Process. 7 (1) (1992) 15–30..
- [4] D. Wang, C.C. Berndt, in: S. Blum-Sandmeier, H. Eschnauer, P. Huber, A.R. Nicol (Eds.), 2nd Plasma-technik-Symposium, vol. 1, June 5–7, 1991. Plasmatechnik AG, Wohlen, Switzerland, pp. 295–304.
- [5] S.Ch. Gill, Ph.D. Thesis, University of Cambridge, 1991.
- [6] R.A. Miller, J. Am. Ceram. Soc. 67 (8) (1984) 517–521..
- [7] N. Birks, G.H. Meier, in: Introduction to High Temperature Oxidation of Metals, Edward Arnold, London, 1983, pp. 92–130.
- [8] C.-C. Chiu, Mater. Sci. Eng. A 150 (1992) 139–148..
- [9] S. Kuroda, T. Fukushima, S. Kitahara, Thin Solid Films 164 (1988) 157–163..
- [10] D.J. Greving, E.F. Rybicki, J.R. Shadley, in C.C. Berndt, S. Sampath (Eds.), Thermal Spray Industrial Applications, ASM International, Materials Park, OH, 1994, pp. 647–653.
- [11] C.K. Lin, C.C. Berndt, in: C.C. Berndt, T.F. Bernecki (Eds.), Thermal Spray Deposits: Research, Design and Applications, ASM International, Materials Park, OH, pp. 561–568.
- [12] C.C. Berndt, H. Herman, Ceram. Eng. Sci. Process. 4 (9) (1983) 792–801..
- [13] C.K. Lin, C.C. Berndt, J. Thermal Spray Technol. 3 (1) (1994) 75–104..